TU Delft

Delft University of Technology

An approach to develop haptic feedback control reference for steering systems using open-loop driving manoeuvres

Chugh, T.; Bruzelius, F.; Klomp, M.; Shyrokau, B.

DOI
10.1080/00423114.2019.1662923

Publication date
2019

Document Version
Final published version

Published in
Vehicle System Dynamics

Citation (APA)
Chugh, T., Bruzelius, F., Klomp, M., & Shyrokau, B. (2019). An approach to develop haptic feedback control reference for steering systems using open-loop driving manoeuvres. *Vehicle System Dynamics*, *58 (2020)*(12), 1953-1976. https://doi.org/10.1080/00423114.2019.1662923

Important note
To cite this publication, please use the final published version (if applicable).
Please check the document version above.

Copyright
Other than for strictly personal use, it is not permitted to download, forward or distribute the text or part of it, without the consent of the author(s) and/or copyright holder(s), unless the work is under an open content license such as Creative Commons.

Takedown policy
Please contact us and provide details if you believe this document breaches copyrights.
We will remove access to the work immediately and investigate your claim.

This work is downloaded from Delft University of Technology.
For technical reasons the number of authors shown on this cover page is limited to a maximum of 10.

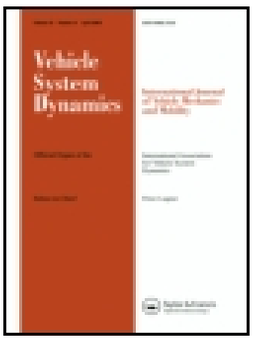

Taylor & Francis
Taylor & Francis Group

Vehicle System Dynamics
International Journal of Vehicle Mechanics and Mobility

ISSN: 0042-3114 (Print) 1744-5159 (Online) Journal homepage: https://www.tandfonline.com/loi/nvsd20

An approach to develop haptic feedback control reference for steering systems using open-loop driving manoeuvres

T. Chugh, F. Bruzelius, M. Klomp & B. Shyrokau

To cite this article: T. Chugh, F. Bruzelius, M. Klomp & B. Shyrokau (2019): An approach to develop haptic feedback control reference for steering systems using open-loop driving manoeuvres, Vehicle System Dynamics, DOI: 10.1080/00423114.2019.1662923

To link to this article: https://doi.org/10.1080/00423114.2019.1662923

© 2019 The Author(s). Published by Informa UK Limited, trading as Taylor & Francis Group

Published online: 10 Sep 2019.

Submit your article to this journal

Article views: 324

View related articles

View Crossmark data

Full Terms & Conditions of access and use can be found at
https://www.tandfonline.com/action/journalInformation?journalCode=nvsd20

VEHICLE SYSTEM DYNAMICS
https://doi.org/10.1080/00423114.2019.1662923

OPEN ACCESS Check for updates

An approach to develop haptic feedback control reference for steering systems using open-loop driving manoeuvres

T. Chugh [a,b], F. Bruzelius[b,c], M. Klomp [a,b] and B. Shyrokau [d]

[a]Volvo Car Corporation, Gothenburg, Sweden; [b]Chalmers University of Technology, Gothenburg, Sweden; [c]Swedish National Road and Transport Research Institute (VTI), Linköping, Sweden; [d]Delft University of Technology, Delft, The Netherlands

ABSTRACT

In this paper, a methodology to capture the model-based haptic feedback control reference for closed-loop steering systems is demonstrated. The parameterisation is based on the measurements of open-loop driving manoeuvres for the inertia-spring-damper-friction reference model. The steady-state and transient manoeuvres are used to identify the model parameters. The reference model is limited to the haptic feedback of driver excitation in the linear vehicle handling range and intended to be used in closed-loop steering control strategies. The model parameters have an intuitive interpretation that allows to be used in both admittance and impedance control setting. The feasibility of the proposed model is demonstrated in a validated simulation environment for electric power assisted steering and on a real hardware for the steer-by-wire force-feedback case.

ARTICLE HISTORY
Received 7 April 2019
Revised 29 June 2019
Accepted 19 August 2019

KEYWORDS
Haptic feedback reference; steering systems; impedance and admittance control; system identification; parameter estimation

1. Introduction

One of the most important features for a typical human–machine interaction is haptic feedback. The term 'haptic' coined from the Greek word '*Haptikos*' meaning a sensation of touch. There has been a lot of research done in this field depending on the application type for the fulfilment of a desired human–machine interface (HMI). For instance, the importance of haptic feedback for a surgeon in robotic surgery is unquestionable. The technical challenge of providing an appropriate force-feedback (FFb) and 'transparency' due to difficulty in modelling the haptic reference (and its quantification) is clearly explained in [1,2]. A typical control architecture involves haptic reference and its feedback controller. For a desired haptic reference, the controller should maintain a balance between the objectives: stability and transparency, see [3] for more details. Other real-time haptic feedback applications, on similar grounds, include flight joystick or yoke control [4], examples of telerobotics [5–8], etc. A common conclusion can be deduced from these case studies that the availability of a relevant haptic feedback is essential for an enhanced human interaction regardless of the machine type.

CONTACT T. Chugh tushar.chugh@volvocars.com

© 2019 The Author(s). Published by Informa UK Limited, trading as Taylor & Francis Group
This is an Open Access article distributed under the terms of the Creative Commons Attribution-NonCommercial-NoDerivatives License (http://creativecommons.org/licenses/by-nc-nd/4.0/), which permits non-commercial re-use, distribution, and reproduction in any medium, provided the original work is properly cited, and is not altered, transformed, or built upon in any way.

The steering system is responsible for the driver–vehicle interaction. A typical steering system has three sources of excitation (for a haptic sensation); driver, environment and vehicle [9]. This paper focuses on the driver excitation and its corresponding haptic response. It means steering motion initiated by the driver, such as turning the vehicle into a corner. For driver excitation, the vehicle reacts according to the given tyre–road grip. This is defined as 'road feedback' in the paper and considered as that part of the haptic feedback which drivers expect while steering, given a certain road surface condition. This definition excludes, for example excitation due to the variation in the tyre–road grip. They are considered as road excitation, caused by the environment. The paper also excludes any reaction from the intervening driving assistance functions, like lane keeping aid, pilot assist and so on, which falls under the vehicle excitation category.

The major shortcoming of a typical electric power assisted steering (EPAS) control for high performance vehicles is its limited potential for transmitting the high frequency road feedback. This is due to a higher effective steering rack or pinion impedance caused by the EPAS motor and its mechanical transmission ratio, see [10, p. 176–189],[11,12]. Similarly in steer-by-wire force-feedback (SbW-FFb), the system bandwidth is affected not only by the motor impedance but also due to uncertainty in the driver arms' impedance [13]. The closed-loop control methods could provide a better hardware impedance compensation, refer [14,15] for EPAS and [13,16–19] for FFb systems. As a result, a reference generator that accurately represents the driver excitation part of the haptic feedback is required.

Common approaches to generate haptic feedback through a reference generator employs a parallel structure. This structure has different steering functions implemented next to each other, for instance in an open-loop regime e.g. [20–25] or impedance (torque) control, e.g. [14,26–28] respectively. Fankem et al. in [23] and Hayama et al. in [24] presented this for SbW-FFb systems. It is an empirical way of implementing the reference generator. A similar approach of implementation is shown in [27], where Lee et al. used vehicle measurements to develop a steering torque map as a function of steering angle, angular velocity and vehicle speed. This approach neglects (steering) inertial torque component, which constitutes the system frequency response. Another aspect not considered in it is the explicit vehicle speed dependence of the haptic feedback. A simplified model-based approach is presented in [25] for a virtual steering feedback, but leaves out the parameterisation procedure of the model. Examples of a simplified model-based admittance (or position-) control reference could be seen in [29–31]. The open-loop EPAS control functions are used with an admittance overlay in [29]. Previous works also lack a thorough frequency response analysis within driver excitation range and mostly compared the on-centre steering response, e.g. [23,25,27,29].

The aim of this paper is to create a model-based haptic feedback reference for closed-loop EPAS and SbW-FFb systems. For building this reference, the vehicle tests were performed on a state-of-the-art (steering rack mounted servo motor) EPAS. A typical EPAS control consists of basic functions (such as power assistance, inertia and friction compensation, active damping and return) and also enhanced functions (e.g. directional stability correction, etc.), see [10, p. 456–466], [20], to ensure a desired steering feel specification as suggested in [14]. In contrast with the typical industrial approach (incorporating the individual function), the steering feel reference could provide a target response during the design stage. Our reference model is obtained by fitting a typical inertia-spring-damper-friction model at different vehicle speeds into the measurement data, thus representing a

desired relationship between torque-to-angle. For this, the standard open-loop (objective steering evaluation) driving manoeuvres were performed, refer [10, p. 161–167], [32] for more details on vehicle tests. These manoeuvres were conducted using a steering robot to exclude the effect of driver arm's time-variant admittance as shown in [33], which was likely to affect the test repeatability. The steering feedback reference model for admittance and impedance control would be the outcome of this paper (although the results qualitatively hold for other closed-loop FFb systems also). In this work, the resulting inertia-spring-damper-friction model represents the cumulative effect of various existing functions (as mentioned before) and hardware to define the haptic feedback reference. The main contribution is the introduction of a model-based approach for a systematic parameterisation with a thorough frequency response investigation. The theory and procedure are discussed in Section 3. The parameter estimation and reference model validation results are given in Section 4.

2. Experimental setup and signal processing

This section briefly describes the experimental setup for system identification and reference model validation, details of the considered open-loop driving manoeuvres and the respective logging of various sensor signals.

For the open-loop manoeuvres, a steering robot aims to follow the reference steering angle, $\delta_{s,ref}$. This is an input to the steering robot controller, which subsequently applies the mechanical input, steering torque, replicating the driver excitation. In the frequency response manoeuvre, the reference angle is linearly excited between 0.2 and 5 Hz over 17.5 s time span. 4–5 Hz frequency approximately represents the maximum periodic steering excitation for humans [34]. In the steady-state manoeuvre, the steering robot aims to follow the sinusoidal $\delta_{s,ref}$ at 0.2 Hz frequency. The excitation amplitude at different vehicle speeds was selected to achieve 3–4 m/s^2 lateral acceleration at 0.2 Hz frequency. For lower vehicle speeds, the lateral acceleration would be less since it is difficult to generate higher lateral forces. The manoeuvres were performed on a flat and dry road surface condition, with minimum variation in the ambient and tyre–road temperature between the different test runs. The test vehicle was equipped with an RT3002 inertial measurement unit (IMU) and GPS. The steering rack force was measured using external tie-rod strain gauges. The internal steering and vehicle signals were logged using the CAN (Controller Area Network). The manoeuvres were performed by the steering robot (SR60 from AB Dynamics). For analysis, the signals were sampled at 100 Hz and synced using a main data acquisition unit. The synchronisation was ensured using the redundant signals from CAN, IMU and steering robot. The list of the sensor signals with their respective source(s) is given in Table 1.

Table 1. Source(s) of vehicle and steering signals for system identification.

Signal name	Source	Signal name	Source
Longitudinal vehicle speed	CAN, IMU, GPS	Steering rack force	Strain gauges
Lateral vehicle speed	IMU, GPS	Steering angle	CAN, steering robot
Lateral acceleration	CAN, IMU	Steering torque	Steering robot
Yaw rate	CAN, IMU	Pinion angle	CAN
Body sideslip angle	IMU	Torsion bar torque	CAN

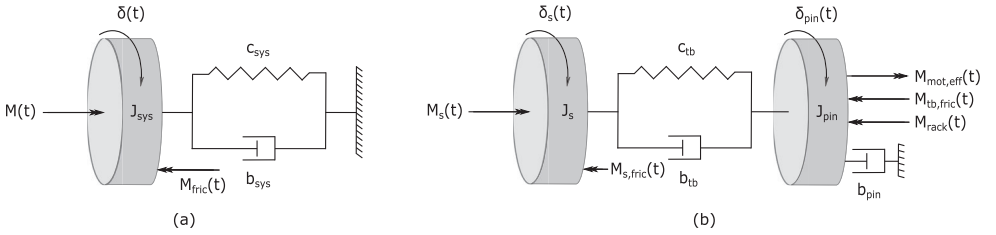

Figure 1. (a) A typical second-order mechanical inertia-spring-damper-friction model. (b) A simplified 2-DOF model of electric power assisted steering system, where M_{rack} represents the moment on the pinion (translated from steering rack force) originated from the vehicle model.

For validation and real-time implementation, an SbW-FFb hardware setup was used. This system was equipped with a direct drive brushless DC motor with an external torque sensor. FFb motor had a rated torque of 7.5 Nm with a resolution of 0.03 Nm; and the encoder for motor angular position had an incremental resolution of 0.009°. The communication between FFb system and dSPACE real-time (DS1006) machine was setup via CAN interface at 1 kHz.

3. Identification of steering feedback for reference generation

The haptic feedback response of a mechanical system is defined in terms of its interaction dynamics [35], i.e. relationship between force and position (or torque and angle). A typical second-order model is shown in Figure 1(a) and defined in Equation (1).Our aim is to objectify the haptic feedback response, δ/M (given a defined model) using inertia (J_{sys}), stiffness (c_{sys}), damping (b_{sys}) and friction (M_{fric}) parameters.

$$J_{\text{sys}}\ddot{\delta}(t) = -b_{\text{sys}}\dot{\delta}(t) - c_{\text{sys}}\delta(t) - M_{\text{fric}}(t) + M(t). \tag{1}$$

3.1. Definition of the reference model

Consider a simplified EPAS system with 2-DOF: steering angle (δ_{s}) and pinion angle (δ_{pin}) in Figure 1(b). The equations of motion are given in Equation (2), such that torsion bar (or pinion) torque is $M_{\text{tb}}(t) = b_{\text{tb}}(\dot{\delta}_{\text{s}}(t) - \dot{\delta}_{\text{pin}}(t)) + c_{\text{tb}}(\delta_{\text{s}}(t) - \delta_{\text{pin}}(t))$. The system inputs are: steering torque, M_{s}, effective motor torque assist, $M_{\text{mot,eff}}$, and equivalent rack torque (or translated rack force on pinion) from the vehicle, M_{rack}. These equations and the model represent the actual steering hardware dynamics. But the reference model is created at the pinion. Therefore, we only consider its dynamics (for identification) and subsequently the relationship between M_{tb} and δ_{pin} is derived. The reason is primarily due to the availability of a torque sensor at this location.

$$\begin{aligned} J_{\text{s}}\ddot{\delta}_{\text{s}}(t) &= -M_{\text{tb}}(t) - M_{\text{s,fric}}(t) + M_{\text{s}}(t), \\ J_{\text{pin}}\ddot{\delta}_{\text{pin}}(t) &= -b_{\text{pin}}\dot{\delta}_{\text{pin}}(t) - M_{\text{rack}}(t) - M_{\text{tb,fric}}(t) + M_{\text{tb}}(t) + M_{\text{mot,eff}}(t). \end{aligned} \tag{2}$$

For pinion dynamics, M_{rack} from the vehicle model defines the steering stiffness. Within linear vehicle handling range (up to 4 m/s^2 lateral acceleration), the single track model is

sufficient to derive M_{rack}. The following relation is used in the pinion moment balance: $M_{\text{rack}} = F_{\text{rack}}/i_{\text{rp}} = f(\alpha_{\text{f}})$, where F_{rack} is the steering rack force, i_{rp} is the rack to pinion gear ratio and α_{f} is the front axle lateral slip angle. The estimation of F_{rack} (or M_{rack}) is further discussed in Section 3.4.2.

The actual motor torque is amplified by the transmission ratio between motor and pinion (i_{epas}), s.t. $M_{\text{mot,eff}} = i_{\text{epas}} M_{\text{mot}}$. The assumed effective motor torque in Equation (3) holds reasonable for controlling the steering pinion (or rack) motion based on the existing steering feedback control functions.

$$M_{\text{mot,eff}}(t) = J_{\text{comp}}\ddot{\delta}_{\text{pin}}(t) + b_{\text{comp}}\dot{\delta}_{\text{pin}}(t) + k_{\text{gain}}M_{\text{tb}}(t) + M_{\text{comp,fric}}(t) \tag{3}$$

$M_{\text{mot,eff}}$ is justified because the steering feedback response is manipulated in terms of inertia, damping, stiffness and friction. J_{comp}, b_{comp} and $M_{\text{comp,fric}}$ represent inertia compensation, active damping and friction compensation terms respectively, primarily as a function of vehicle speed. The effect of basic power assistance (as mentioned in e.g. [14,20,23]) is described by the term k_{gain}. Inserting Equation (3) in the pinion moment balance from Equation (2), the following result can be derived:

$$J_{\text{ref}}\ddot{\delta}_{\text{pin}}(t) = -b_{\text{ref}}\dot{\delta}_{\text{pin}}(t) - M_{\text{rack}}(t) - M_{\text{ref,fric}}(t) + K_{\text{assist}}M_{\text{tb}}(t), \tag{4}$$

where $K_{\text{assist}} = 1 + k_{\text{gain}}$, $J_{\text{ref}} = J_{\text{pin}} - J_{\text{comp}}$, $b_{\text{ref}} = b_{\text{pin}} - b_{\text{comp}}$ and $M_{\text{ref,fric}} = M_{\text{tb,fric}} - M_{\text{comp,fric}}$. Equation (4) is defined as the reference model under identification, s.t. $J_{\text{ref}}\ddot{\delta}_{\text{pin}}(t) + b_{\text{ref}}\dot{\delta}_{\text{pin}}(t) + M_{\text{rack}}(t) = M_{\text{pin,dyn}}(t)$ altogether define system dynamics, K_{assist} represents basic assistance and non-linear friction by $M_{\text{ref,fric}}$. The estimation of M_{rack}, J_{ref}, b_{ref}, K_{assist} and $M_{\text{ref,fric}}$ is discussed further. It should be noted that J_{ref}, b_{ref} and $M_{\text{ref,fric}}$ although have a physical meaning, but they represent a cumulative effect of the EPAS control software and hardware dynamics.

3.2. Reference generator for admittance and impedance control

In admittance control, M_{tb} sensor signal generates the reference angular position ($\delta_{\text{pin,ref}}$) and velocity ($\dot{\delta}_{\text{pin,ref}}$) for the feedback control. The reference layout is shown in Figure 2(a). The system dynamics block contains the pinion response based on the estimated road feedback, refer Equation (4). The effective torsion bar torque is an output of the basic assist (which represents an amplification of M_{tb}), s.t. $M_{\text{tb,eff}} = K_{\text{assist}}M_{\text{tb}}$. The non-linear friction torque (as a function of $\dot{\delta}_{\text{pin,ref}}$) is fed back to $M_{\text{tb,eff}}$.

The reference generator for impedance control is complementary to admittance control, refer Figure 2(b). The inverse system dynamics is theoretically improper. For practical realisation, this is prevented by filtering and estimation to obtain the pinion angular acceleration for an appropriate inertial torque component. Hence, both sensor signals δ_{pin} and $\dot{\delta}_{\text{pin}}$ are used in this block. The output dynamic pinion moment is merged with the torque from the feedforward non-linear friction model. The resulting $M_{\text{tb,eff}}$ is then taken as an input to the inverse basic assistance for generating the reference torque signal, $M_{\text{tb,ref}}$. This reference model can also be used for the open loop architecture (without feedback control) in FFb systems, as discussed in [13].

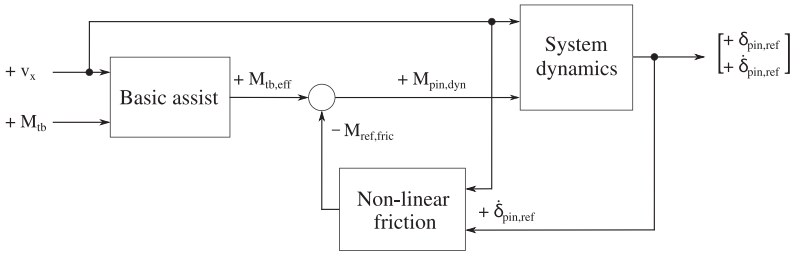

(a) Reference generator for admittance control

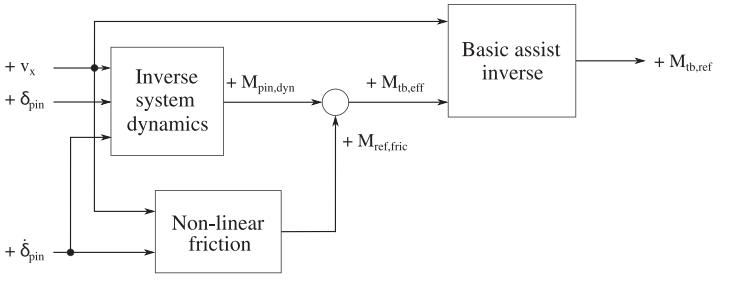

(b) Reference generator for impedance control

Figure 2. Reference generator architecture for (a) admittance and (b) impedance control respectively. System dynamics (and its inverse) contains the pinion frequency response. Basic assist (and its inverse) describes a quasi-static relationship between the rack force (or equivalently rack torque) and torsion bar torque. Non-linear friction represents the pinion Coulomb friction dynamics creating a hysteresis effect.

3.3. Overview of the identification scheme

The flow chart in Figure 3 briefly describes the identification procedure for generating the steering feedback reference model from the given vehicle measurements. The first step is to identify the steering rack force frequency response function (FRF), i.e. $F_{\text{rack}}/x_{\text{rack}}$ (or equivalently M_{rack} in Equation 4) using the single track vehicle model. To ensure the model identifiability as a necessary condition, this step is subdivided into two parts: (a) vehicle and tyre parameters estimation using IMU signals ($\dot{\psi}$, a_y and β) and (b) steering trail estimation using the measured F_{rack} signal. Once the steering rack force FRF is available, then the pinion moment balance (of the steering model) is used in the next two steps. The parameters J_{ref} and b_{ref}, in Equation (4), are estimated at first using the measured $\delta_{\text{pin}}/M_{\text{tb}}$ FRF. And finally the basic assistance function, K_{assist}, and the non-linear Coulomb friction, $M_{\text{ref,fric}}$, are estimated using the steady-state steering response.

3.4. Frequency response

The frequency response manoeuvre is performed to estimate the linearised system parameters. For higher excitation amplitudes (within sliding friction region), the non-linear (Coulomb) friction does not affect the FRF estimate [36]. As a result, the (physical) friction contribution can be disregarded from Equation (1). The primary aspects for a dynamic system are: eigenfrequency (ω_{e}) and damping ratio (D_{e}). The system eigenfrequency depends on c_{sys} and J_{sys}, s.t. $\omega_{\text{e}} = \sqrt{c_{\text{sys}}/J_{\text{sys}}}$. Whereas, the damping ratio is given

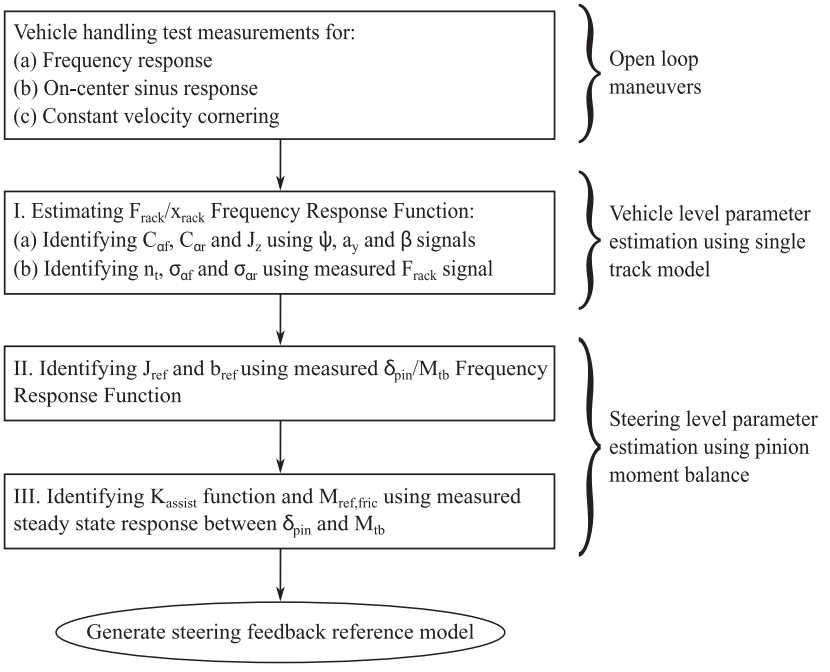

Figure 3. An overview of the system identification procedure for generating the steering feedback reference model. Step I is used for estimating the vehicle model parameters. The steering model parameters are estimated in Steps II and III.

as $D_e = b_{sys}/(2J_{sys}\omega_e)$. For a given input–output system response, these parameters are estimated to fit an inertia-spring-damper model to the given response. In conventional steering systems, the haptic feedback (defined in the terms of torque to angle relationship) with driver excitation depends on the vehicle and tyre response. This is because the tyre self-aligning moment and mechanical steer torque generate the required steering rack force about the steering axis, which acts as a stiffness especially at higher vehicle speeds. In the first step, the unknown vehicle model parameters are identified. Once the steering rack force response from the vehicle is known, the steering related inertia and damping can be estimated as shown in Figure 3. This is further discussed in Sections 3.4.2 and 3.4.3 respectively.

3.4.1. Data post-processing

The direct approach to the closed-loop system identification is performed as proposed in [37, p. 434–452]. The measured (disturbance) signal 'M_s' is used for generating the spectral densities. The multiple frequency response test runs were combined together (on the time scale) during post-processing to create a single persistently excited disturbance and reference signal, because it was difficult to perform a long continuous excitation at higher vehicle speeds due to the test track limitation.

The FRF estimate assumes an LTI system. The estimates are marked using '$\wedge$' notation. The sampled signals are Fourier transformed to estimate the disturbance-input and disturbance-output cross-spectral densities, $\hat{S}_{du}(i\omega)$ and $\hat{S}_{dy}(i\omega)$ respectively, using the

complex conjugate disturbance $M_s^*(i\omega)$. The estimated cross- and power-spectral densities are averaged for three consecutive frequencies to reduce the variance, thus creating a new frequency vector ω_n. The input–output FRF, $\hat{H}_{uy}(i\omega_n)$, in Equation (5) is defined as the ratio between $\hat{S}_{dy}(i\omega_n)$ and $\hat{S}_{du}(i\omega_n)$. A detailed explanation of the frequency response analysis can be found in [37, p. 170–189]. During parameter estimation, only high coherence estimates ($\hat{\gamma}_{dx} > 0.85$ for a given signal 'x'), as defined in Equation (5), are selected. This is to emphasise the system linearity and less distortion by the sensor noise.

$$\begin{aligned} \hat{S}_{du}(i\omega) &= M_s^*(i\omega)U(i\omega), \quad \hat{S}_{dy}(i\omega) = M_s^*(i\omega)Y(i\omega), \\ \hat{H}_{uy}(i\omega_n) &= \frac{\hat{S}_{dy}(i\omega_n)}{\hat{S}_{du}(i\omega_n)} \quad \text{and} \quad \hat{\gamma}_{dx}^2(\omega_n) = \frac{|\hat{S}_{dx}(i\omega_n)|^2}{\hat{S}_{dd}(i\omega_n)\hat{S}_{xx}(i\omega_n)}. \end{aligned} \tag{5}$$

3.4.2. Estimation of steering rack force as a function of rack displacement

The offline estimation of the required vehicle parameters was performed for F_{rack}. Assuming LTI single track vehicle model at a known constant longitudinal vehicle speed, v_x, the system state–space matrices are given as follows.

$$\mathbf{A} = \begin{bmatrix} 0 & -v_x & \frac{C_{\alpha_\text{f}}}{m} & \frac{C_{\alpha_\text{r}}}{m} \\ 0 & 0 & \frac{C_{\alpha_\text{f}} l_\text{f}}{J_z} & \frac{-C_{\alpha_\text{r}} l_\text{r}}{J_z} \\ \frac{-1}{\sigma_{\alpha_\text{f}}} & \frac{-l_\text{f}}{\sigma_{\alpha_\text{f}}} & \frac{-v_x}{\sigma_{\alpha_\text{f}}} & 0 \\ \frac{-1}{\sigma_{\alpha_\text{r}}} & \frac{l_\text{r}}{\sigma_{\alpha_\text{r}}} & 0 & \frac{-v_x}{\sigma_{\alpha_\text{r}}} \end{bmatrix}, \quad \mathbf{B} = \begin{bmatrix} 0 \\ 0 \\ \frac{v_x}{\sigma_{\alpha_\text{f}}} \\ 0 \end{bmatrix},$$

$$\mathbf{C} = \begin{bmatrix} 0 & 1 & 0 & 0 \\ 0 & 0 & \frac{C_{\alpha_\text{f}}}{m} & \frac{C_{\alpha_\text{r}}}{m} \\ \frac{1}{v_x} & 0 & 0 & 0 \end{bmatrix} \quad \text{and}$$

$$\mathbf{D} = \mathbf{0}_{3\times 1}. \tag{6}$$

The state variables are lateral vehicle speed, yaw rate, front and rear axle lateral slip angle, $\mathbf{x} = [v_y \ \dot{\psi} \ \alpha_\text{f} \ \alpha_\text{r}]^\text{T}$; and the input is road wheel angle, $\mathbf{u} = \delta_\text{tyre}$. The output measured variables are yaw rate, lateral acceleration and body sideslip angle, s.t. $\mathbf{y} = [\dot{\psi} \ a_y \ \beta]^\text{T}$. Using small angle approximation, the linear relation $\beta = v_y/v_x$ holds. The known parameters include vehicle mass (m), distance from the front and rear axle to vehicle's centre of gravity (l_f, l_r). The unknown parameters include axle tyre cornering stiffness, C_{α_f} and C_{α_r}, vehicle yaw inertia (J_z) and tyre relaxation length ($\sigma_{\alpha_\text{f}}, \sigma_{\alpha_\text{r}}$). δ_tyre is assumed as linearly related to δ_pin via the steering ratio (i_s), $\delta_\text{tyre} = \delta_\text{pin}/i_\text{s}$. The ratio i_s is assumed as a constant by neglecting the effects of wheel kinematics. Also, the steering rack position is linearly related to δ_pin, s.t. $x_\text{rack} = \delta_\text{pin}/i_\text{rp}$.

The unknown parameter vector is defined as $\boldsymbol{\theta}(v_x) = [C_{\alpha_\text{f}} \ C_{\alpha_\text{r}} \ \sigma_{\alpha_\text{f}} \ \sigma_{\alpha_\text{r}} \ J_z]^\text{T}$ for the estimation. The optimisation problem minimises the objective function, $J(\boldsymbol{\theta})$, using the

least-squares criterion as follows:

$$\begin{aligned} \min_{\boldsymbol{\theta}} \quad & (\mathbf{W}_\mathrm{m}\mathbf{N}_\mathrm{m}\mathbf{E}_\mathrm{m} + \mathbf{W}_\mathrm{p}\mathbf{N}_\mathrm{p}\mathbf{E}_\mathrm{p}) = J(\hat{\boldsymbol{\theta}}), \\ \text{subject to} \quad & \boldsymbol{\theta}^- < \boldsymbol{\theta} < \boldsymbol{\theta}^+, \end{aligned} \tag{7}$$

where

$$\begin{aligned} \mathbf{W}_\mathrm{m} &= [w_{\mathrm{mag},\dot{\psi}} \quad w_{\mathrm{mag},a_y} \quad w_{\mathrm{mag},\beta}], \quad \mathbf{W}_\mathrm{p} = [w_{\mathrm{ang},\dot{\psi}} \quad w_{\mathrm{ang},a_y} \quad w_{\mathrm{ang},\beta}], \\ \mathbf{N}_\mathrm{m} &= \mathrm{diag}\big([1/\hat{H}_{\mathrm{stat},\delta\dot{\psi}} \quad 1/\hat{H}_{\mathrm{stat},\delta a_y} \quad 1/\hat{H}_{\mathrm{stat},\delta\beta}]\big), \quad \mathbf{N}_\mathrm{p} = 1/\pi\ \mathbf{I}_{3\times 3}, \\ \mathbf{E}_\mathrm{m} &= \frac{1}{n}\begin{bmatrix} \sum_n (|\hat{H}_{\delta\dot{\psi}}(i\omega_n)| - |H_{\delta\dot{\psi}}(i\omega_n)|)^2 \\ \sum_n (|\hat{H}_{\delta a_y}(i\omega_n)| - |H_{\delta a_y}(i\omega_n)|)^2 \\ \sum_n (|\hat{H}_{\delta\beta}(i\omega_n)| - |H_{\delta\beta}(i\omega_n)|)^2 \end{bmatrix} \quad \text{and} \\ \mathbf{E}_\mathrm{p} &= \frac{1}{n}\begin{bmatrix} \sum_n (\angle\hat{H}_{\delta\dot{\psi}}(i\omega_n) - \angle H_{\delta\dot{\psi}}(i\omega_n))^2 \\ \sum_n (\angle\hat{H}_{\delta a_y}(i\omega_n) - \angle H_{\delta a_y}(i\omega_n))^2 \\ \sum_n (\angle\hat{H}_{\delta\beta}(i\omega_n) - \angle H_{\delta\beta}(i\omega_n))^2 \end{bmatrix}. \end{aligned} \tag{8}$$

The weighting matrices $\mathbf{W}_\mathrm{m}$ and $\mathbf{W}_\mathrm{p}$ consist of weighting gains, s.t. $\sum w_{\mathrm{mag},y_k} = 1$ and $\sum w_{\mathrm{ang},y_k} = 1$. These gains correspond to the error in magnitude and phase response of the three input–output FRF respectively, yaw rate, lateral acceleration and sideslip angle. The resulting mean square error in each ($\mathbf{E}_\mathrm{m}$ and $\mathbf{E}_\mathrm{p}$) has been normalised with $\mathbf{N}_\mathrm{m}$ and $\mathbf{N}_\mathrm{p}$ respectively. For magnitude, it is normalised with respect to its estimated steady-state gain $\hat{H}_{\mathrm{stat},\delta y_k}$ at 0.2 Hz, whereas π for the phase delay as defined in Equation (8).

The estimation of steering rack force as a function of rack displacement is solved in three steps by non-linear constrained optimisation. At first, the low frequency response (<0.5 Hz) corresponding to the steady-state vehicle behaviour is used for the estimation of C_{α_f} and C_{α_r}. Since the effect of phase delay is not significant for lower frequencies, hence $\mathbf{W}_\mathrm{p} = \mathbf{0}_{1\times 3}$. $\hat{C}_{\alpha_\mathrm{f}}$ and $\hat{C}_{\alpha_\mathrm{r}}$ were then verified by performing a constant velocity cornering manoeuvre. It is performed at lower (and constant) steering angular velocity. The assumption of linear tyre characteristic holds true for lower slip angles and previously mentioned lateral acceleration range. In the second step, the transient parameters $\sigma_{\alpha_\mathrm{f}}, \sigma_{\alpha_\mathrm{r}}$ and J_z are estimated for the entire frequency response by using $\hat{C}_{\alpha_\mathrm{f}}$ and $\hat{C}_{\alpha_\mathrm{r}}$ from the previous step. The weighting gains are selected to have an acceptable yaw rate, lateral acceleration and sideslip angle response of the fitted model at respective vehicle speeds. A good correlation of $\beta/\delta_\mathrm{tyre}$ and a_y/δ_tyre FRF was found essential for the steering rack force estimation, since $F_\mathrm{rack} = f(\alpha_\mathrm{f})$ as given in Equation (9). Another crucial point, the magnitude of $\hat{\sigma}_{\alpha_\mathrm{f}}$ and $\hat{\sigma}_{\alpha_\mathrm{r}}$ obtained in this step was higher ($\approx$1 m) than reported in the literature. This might be due to the effect of un-modelled dynamics being propagated in the results, such as latency in vehicle CAN signals. As a result, with these values the further steps were difficult to correlate to the measured FRF. Hence, they are estimated again using the measured signal

of steering rack force from the strain gauges in the last step. The parameter estimation vector is $\boldsymbol{\theta}(v_x) = [n_t\ \sigma_{\alpha_\mathrm{f}}\ \sigma_{\alpha_\mathrm{r}}]^\mathrm{T}$, where n_t is the steering trail (sum of caster and tyre pneumatic trail). The low frequency response (<0.5 Hz) is used for the estimation of n_t; and then the entire frequency response for $\sigma_{\alpha_\mathrm{f}}$ and $\sigma_{\alpha_\mathrm{r}}$. The optimisation problem is solved similar to above. It minimises the error in magnitude and phase of the rack force FRF in Equation (9), normalised with the estimated steady-state gain and π respectively. If the derived $F_\mathrm{rack}/x_\mathrm{rack}$ FRF is comparable to the measured FRF, then the estimation holds correct for Step I in Figure 3.

$$\frac{F_\mathrm{rack}(i\omega_n)}{x_\mathrm{rack}(i\omega_n)} = \left(\hat{C}_{\alpha_\mathrm{f}} n_t \frac{i_\mathrm{rp}^2}{i_\mathrm{s}^2}\right) \frac{\alpha_\mathrm{f}(i\omega_n)}{\delta_\mathrm{tyre}(i\omega_n)} \tag{9}$$

3.4.3. Estimation of reference pinion inertia and damping

The second step of this frequency response analysis (see Figure 3) is to estimate the reference pinon inertia and viscous damping in Equation (4), using the estimated rack force response from the previous section. These unknown parameters are J_ref and b_ref respectively. Typically, k_gain is a non-linear function which is further discussed in Section 3.5.1. However for an LTI models' FRF, k_gain becomes linearised parameter.

Using Equations (4), (6) and (9) by neglecting friction dynamics, the updated system state–space matrices become as Equation (10). The state, output and input vectors are as follows: $\mathbf{x} = [\delta_\mathrm{pin}\ \dot{\delta}_\mathrm{pin}\ v_y\ \dot{\psi}\ \alpha_\mathrm{f}\ \alpha_\mathrm{r}]^\mathrm{T}$, $\mathbf{y} = [\delta_\mathrm{pin}\ \dot{\delta}_\mathrm{pin}]^\mathrm{T}$ and $\mathbf{u} = M_\mathrm{tb}$ respectively.

$$\mathbf{A} = \begin{bmatrix} 0 & 1 & 0 & 0 & 0 & 0 \\ \dfrac{-\hat{C}_{\alpha_\mathrm{f}}\hat{n}_t}{i_\mathrm{s}^2 J_\mathrm{ref}} & \dfrac{-b_\mathrm{ref}}{J_\mathrm{ref}} & \dfrac{\hat{C}_{\alpha_\mathrm{f}}\hat{n}_t}{i_\mathrm{s} J_\mathrm{ref} v_x} & \dfrac{\hat{C}_{\alpha_\mathrm{f}} l_\mathrm{f} \hat{n}_t}{i_\mathrm{s} J_\mathrm{ref} v_x} & 0 & 0 \\ 0 & 0 & 0 & -v_x & \dfrac{\hat{C}_{\alpha_\mathrm{f}}}{m} & \dfrac{\hat{C}_{\alpha_\mathrm{r}}}{m} \\ 0 & 0 & 0 & 0 & \dfrac{\hat{C}_{\alpha_\mathrm{f}} l_\mathrm{f}}{\hat{J}_z} & \dfrac{-\hat{C}_{\alpha_\mathrm{r}} l_\mathrm{r}}{\hat{J}_z} \\ \dfrac{v_x}{i_\mathrm{s}\hat{\sigma}_{\alpha_\mathrm{f}}} & 0 & \dfrac{-1}{\hat{\sigma}_{\alpha_\mathrm{f}}} & \dfrac{-l_\mathrm{f}}{\hat{\sigma}_{\alpha_\mathrm{f}}} & \dfrac{-v_x}{\hat{\sigma}_{\alpha_\mathrm{f}}} & 0 \\ 0 & 0 & \dfrac{-1}{\hat{\sigma}_{\alpha_\mathrm{r}}} & \dfrac{l_\mathrm{r}}{\hat{\sigma}_{\alpha_\mathrm{r}}} & 0 & \dfrac{-v_x}{\hat{\sigma}_{\alpha_\mathrm{r}}} \end{bmatrix}, \quad \mathbf{B} = \begin{bmatrix} 0 \\ \dfrac{1+k_\mathrm{gain}}{J_\mathrm{ref}} \\ 0 \\ 0 \\ 0 \\ 0 \end{bmatrix},$$

$$\mathbf{C} = \begin{bmatrix} \mathbf{I}_{2\times 2} & \mathbf{0}_{2\times 4} \end{bmatrix} \quad \text{and} \quad \mathbf{D} = \mathbf{0}_{2\times 1}. \tag{10}$$

The unknown parameter vector is $\boldsymbol{\theta}(v_x) = [J_\mathrm{ref}\ b_\mathrm{ref}\ k_\mathrm{gain}]^\mathrm{T}$. Again, the optimisation problem minimises the objective function in Equation (7). The weighting gains in $\mathbf{W}_\mathrm{m}$ and $\mathbf{W}_\mathrm{p}$ are selected with the same criteria as mentioned before. The two input–output FRF are $\delta_\mathrm{pin}/M_\mathrm{tb}$ and $\dot{\delta}_\mathrm{pin}/M_\mathrm{tb}$. The mean square normalised error is chosen for both magnitude and phase in the objective matrices ($\mathbf{E}_\mathrm{m}$ and $\mathbf{E}_\mathrm{p}$) as shown below:

$$\mathbf{W}_\mathrm{m} = [w_{\mathrm{mag},\delta_\mathrm{pin}} \quad w_{\mathrm{mag},\dot{\delta}_\mathrm{pin}}], \quad \mathbf{W}_\mathrm{p} = [w_{\mathrm{ang},\delta_\mathrm{pin}} \quad w_{\mathrm{ang},\dot{\delta}_\mathrm{pin}}], \quad \mathbf{N}_\mathrm{m} = \mathbf{N}_\mathrm{p} = \mathbf{I}_{2\times 2},$$

$$\mathbf{E}_{\mathrm{m}} = \frac{1}{n}\begin{bmatrix} \sum_n ((|\hat{H}_{M\delta}(i\omega_n)| - |H_{M\delta}(i\omega_n)|)/\hat{H}_{\mathrm{stat},M\delta})^2 \\ \sum_n ((|\hat{H}_{M\dot{\delta}}(i\omega_n)| - |H_{M\dot{\delta}}(i\omega_n)|)/\hat{H}_{\mathrm{stat},M\dot{\delta}})^2 \end{bmatrix} \quad \text{and}$$

$$\mathbf{E}_{\mathrm{p}} = \frac{1}{n}\begin{bmatrix} \sum_n ((\angle\hat{H}_{M\delta}(i\omega_n) - \angle H_{M\delta}(i\omega_n))/\pi)^2 \\ \sum_n ((\angle\hat{H}_{M\dot{\delta}}(i\omega_n) - \angle H_{M\dot{\delta}}(i\omega_n))\ 2/\pi)^2 \end{bmatrix}. \tag{11}$$

The optimisation is performed in a similar fashion as before, the error in magnitude and phase are normalised with its steady-state gain and absolute peak phase. The final solution provides $\hat{J}_{\mathrm{ref}}$, $\hat{b}_{\mathrm{ref}}$ and $\hat{k}_{\mathrm{gain}}$ at different v_x, thus characterising the FRF estimate of the haptic feedback. The validation results are shown in Section 4.

3.5. Steady-state response

The steady-state steering response is used to estimate the non-linear parameters: basic assistance and Coulomb friction, refer Step III in Figure 3. Equation (4) is rewritten as

$$\hat{J}_{\mathrm{ref}}\ddot{\delta}_{\mathrm{pin}}(t) = -\hat{b}_{\mathrm{ref}}\dot{\delta}_{\mathrm{pin}}(t) - \hat{F}_{\mathrm{rack}}(t)/i_{\mathrm{rp}} - M_{\mathrm{ref,fric}}(t) + K_{\mathrm{assist}}M_{\mathrm{tb}}(t). \tag{12}$$

The reference friction torque, $M_{\mathrm{ref,fric}}$, is the resulting pinion friction (effectively on the steering rack) and not the actual hardware friction, because of the friction compensation in Equation (3). The following sections explain a step-wise estimation procedure for K_{assist} and $M_{\mathrm{ref,fric}}$.

3.5.1. Estimation of non-linear basic assistance

The first part is to estimate the non-linear steering stiffness that the driver experiences during steady-state cornering within the linear range of the tyre and vehicle. Typically, the basic assistance defines the motor assist torque as a function of torsion bar torque [10,20]. Alternatively, it could be seen as a steering rack force filtering functionality as presented in [23,25]. These curves are finally tuned empirically on the vehicle level at different speeds by experts. The main purpose is to achieve an appropriate steering feedback, especially for low frequency excitation.

The linear handling range can be seen in Figure 4(b), as the rack force is linearly related to the rack displacement at a given v_x. The estimated steady-state stiffness $\hat{c}_{\mathrm{rack}}$ is derived from Section 3.4.2 at 0.2 Hz frequency. The corresponding pinion response is shown in Figure 4(a). Although the system stiffness is linear, the drivers consider this motor assist generated non-linear steering characteristic as a 'good' steering feel. The steady-state steering response can be further segregated to three domains: on-centre, transition and off-centre, refer Figure 4(a). The on-centre stiffness ($c_{\mathrm{pin,on}}$) directly correlates to the steering rack stiffness ($\hat{c}_{\mathrm{pin,on}} = \hat{c}_{\mathrm{rack}}/i_{\mathrm{rp}}^2$), as drivers prefer to feel the actual road at zero front axle tyre slip angle. With increasing rack force, $c_{\mathrm{pin,on}}$ transitions to off-centre stiffness $c_{\mathrm{pin,off}}$.

The proposed Gaussian function in Equation (13) defines this transition, where σ is a model fitting parameter. It was first proposed in [25], but suitably modified here for a more precise result. Here, c_{pin} is considered to be a non-linear function in M_{tb} rather than

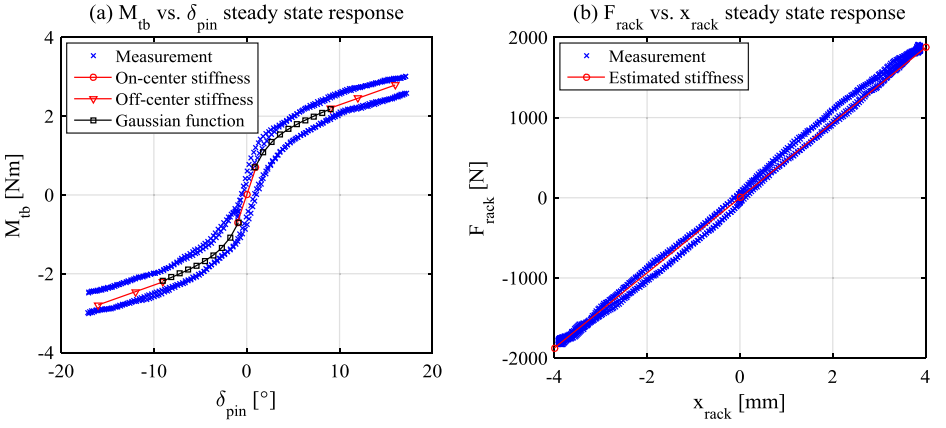

Figure 4. Steady-state steering response at $v_x = 90$ km/h with (a) torsion bar torque versus pinion angle. The on-centre pinon stiffness is directly related to the steering rack stiffness. The transition from on- to off-centre stiffness is modelled using the Gaussian function. (b) The linear behaviour occurs for steering rack force versus rack displacement plot. The estimated stiffness from the frequency response section (at 0.2 Hz) correlates with the actual measurement as shown above.

α_f (or F_{rack}) as proposed in [25]. The advantage of this approach is that c_{pin} saturates to $c_{pin,off}$ ($\neq 0$ Nm/rad) as a more realistic solution within the given steering operational range. Whereas in the other case c_{pin} saturates to 0 Nm/rad much faster (at very low F_{rack}), thus deviating from the reality. The disadvantage of this approach is that $c_{pin,off}$ never saturates to 0 Nm/rad, and thus not valid for a very high F_{rack} or a_y range because typically the basic assist curves saturate with increasing F_{rack}, s.t. $c_{pin,off} \to 0$ Nm/rad. Therefore for higher rack force applications during the development process, it is more sensible to use the actual basic assistance function.

$$\delta_{pin} = \frac{M_{tb}}{c_{pin}(f(M_{tb}))} = \frac{M_{tb}}{(c_{pin,on} - c_{pin,off})e^{-\frac{M_{tb}^2}{2\sigma^2}} + c_{pin,off}}. \tag{13}$$

Using Equation (12) by neglecting friction and pinion dynamics, Equation (13) and $F_{rack}/i_{rp} = c_{pin,on}\delta_{pin}$, K_{assist} can be derived as follows:

$$K_{assist} = \left[\left(1 - \frac{c_{pin,off}}{c_{pin,on}}\right)e^{-M_{tb}^2/2\sigma^2} + \frac{c_{pin,off}}{c_{pin,on}}\right]^{-1}. \tag{14}$$

The parameter under estimation is $c_{pin,off}$, given $\hat{c}_{pin,on}$ and a pre-selected σ. Using the actual δ_{pin} signal, the quadratic error function in M_{tb} is minimised to determine K_{assist}, s.t. $M_{tb}(t) = K_{assist}^{-1}\hat{c}_{pin,on}\delta_{pin}(t)/i_{rp}$. The result obtained from this provides the non-linear stiffness function (i.e. a quasi-static relationship between M_{tb} and $M_{tb,eff}$ as shown in Figure 2a). This parameter is not responsible for the steering hysteresis.

3.5.2. Estimation of non-linear friction

The last part of the identification scheme is non-linear friction. The pinion friction is parameterised using a Dahl friction model, see e.g. [38]. It considers the friction as a

function of both the displacement and velocity, where c_{fric} is defined as the stiffness parameter at $M_{\text{ref,fric}} = 0$. The maximum friction torque is bounded by the Coulomb friction, $M_{\text{fric,C}}$. The simplified 'Dahl model' differential equation is shown in Equation (15), with the unknown parameters c_{fric} and $M_{\text{fric,C}}$. However, the implementation of a good friction model requires high c_{fric} values, which is difficult to obtain on a real-time machine due to very high numerical stiffness of the discretised model. Therefore this parameter is constrained by its practical implication and thus fittingly pre-selected for estimating $M_{\text{fric,C}}$ only.

$$\dot{M}_{\text{ref,fric}}(t) = c_{\text{fric}}\dot{\delta}_{\text{pin}}(t) - \frac{M_{\text{ref,fric}}(t)}{M_{\text{fric,C}}} c_{\text{fric}}|\dot{\delta}_{\text{pin}}(t)|. \tag{15}$$

The pinion moment balance in Equation (12) can be suitably modified to Equation (16) as follows:

$$M_{\text{tb}}(t) = K_{\text{assist}}^{-1}(M_{\text{ref,fric}}(t) + \hat{M}_{\text{pin,dyn}}(t)), \tag{16}$$

where $\hat{M}_{\text{pin,dyn}} = \hat{J}_{\text{ref}}\ddot{\delta}_{\text{pin}} + \hat{b}_{\text{ref}}\dot{\delta}_{\text{pin}} + \hat{F}_{\text{rack}}/i_{\text{rp}}$. For steady-state, the contribution of $\hat{J}_{\text{ref}}\ddot{\delta}_{\text{pin}}$ is negligible; hence it is excluded in the estimation of $M_{\text{ref,fric}}$. Using Equation (15), already estimated parameters, available signals δ_{pin} and $\dot{\delta}_{\text{pin}}$, M_{tb} in Equation (16) are computed at each time step. Finally, the squared error in M_{tb} is minimised to estimate $M_{\text{fric,C}}$ at different v_x. This part captures the effect of steering hysteresis.

4. Results

This section has been divided into two parts. At first, the results of the parameter estimation from Sections 3.4 and 3.5 are discussed. Then the validation results for the admittance and impedance reference, see Figure 2, are presented. For EPAS, the simulations were implemented in CarMaker. Whereas for SbW-FFb system, the results were experimentally obtained.

4.1. Parameter estimation

The frequency response results of Section 3.4.2 are shown in Figures 5 and 6 for vehicle speeds 90 and 75 km/h respectively. The tyre and vehicle parameters estimation are based on $\dot{\psi}/\delta_{\text{tyre}}$, a_y/δ_{tyre} and $\beta/\delta_{\text{tyre}}$ frequency response. Figure 5 shows a good correlation between the measurement data and fitted model. The FRF estimate of $F_{\text{rack}}/x_{\text{rack}}$ can be seen in Figure 6. This result corresponds to Equation (9). The comparison with the actual measurement shows marginal deviation around 1 Hz. The two possibilities, out of many others, could be either disregarding some actual dynamics or the location of rack force strain gauges on the tie-rods. $\hat{F}_{\text{rack}}/x_{\text{rack}}$ response is used for the estimation of reference pinion inertia and damping in the next step.

The pinion response in terms of torsion bar torque to pinion angle and angular velocity FRF for 90 and 75 km/h is presented in Figure 7. The first peak identified in $\delta_{\text{pin}}/M_{\text{tb}}$ around 1.5 Hz is due to rack force response, eigenfrequency caused by the vehicle yaw motion. The second peak as observed in $\dot{\delta}_{\text{pin}}/M_{\text{tb}}$ at approximately 4 Hz is caused by the pinion (or steering rack) motion. The fitted inertia-spring-damper FRF shows a good

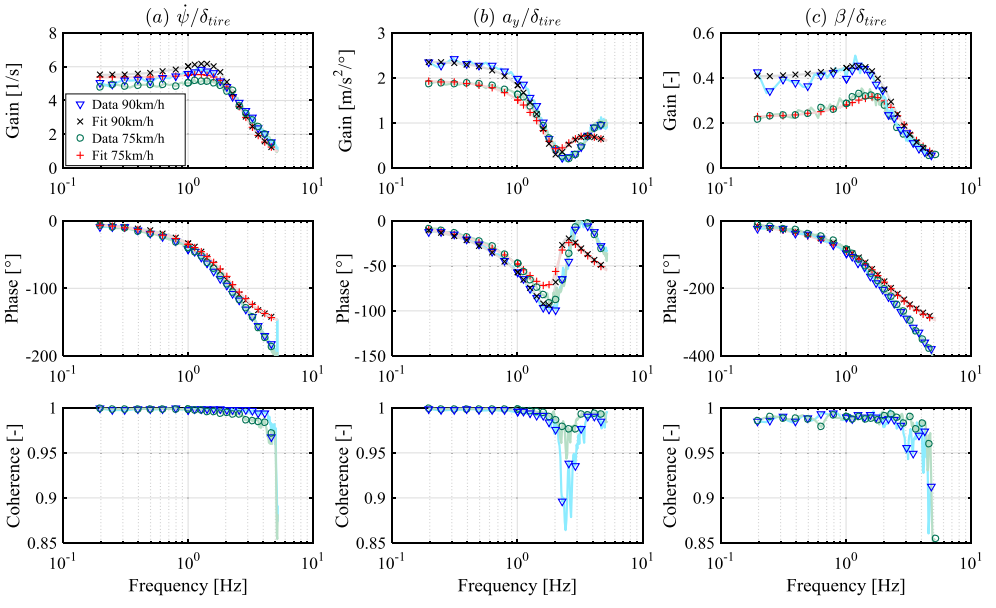

Figure 5. Frequency response of vehicle at $v_x = 90$ and 75 km/h. The plots exhibit tyre angle to (a) yaw rate, (b) lateral acceleration and (c) sideslip angle frequency response respectively. The measured FRF's quality is determined by the coherence plots.

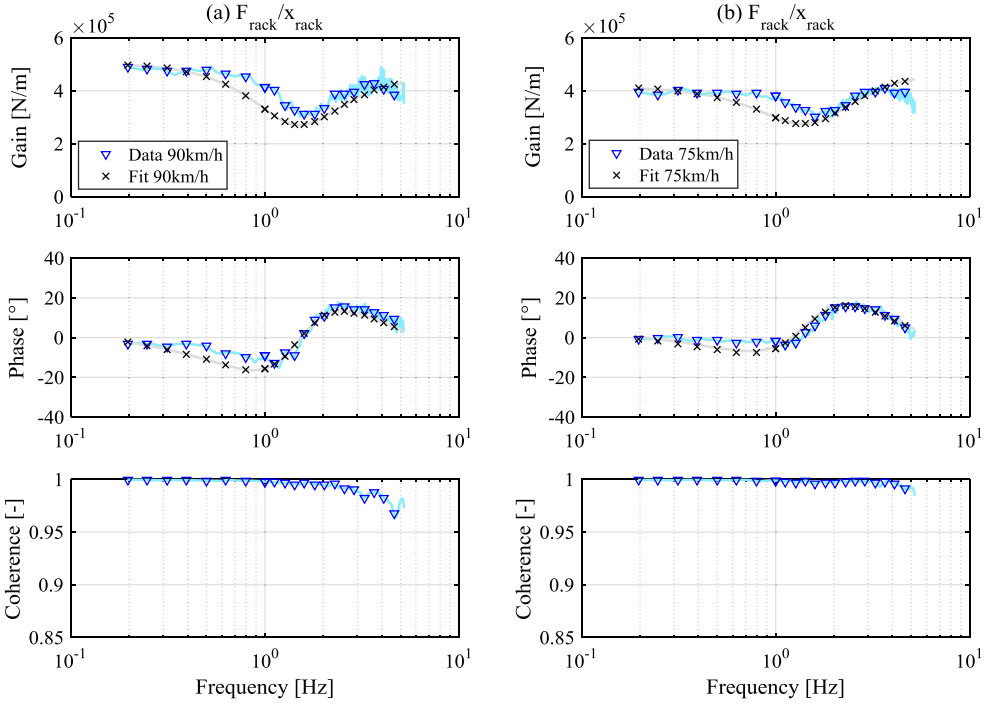

Figure 6. Frequency response of steering rack at $v_x = 90$ km/h (a) and 75 km/h (b) respectively. The plots show FRF estimate of $F_{\text{rack}}/x_{\text{rack}}$ for the test data and fitted model.

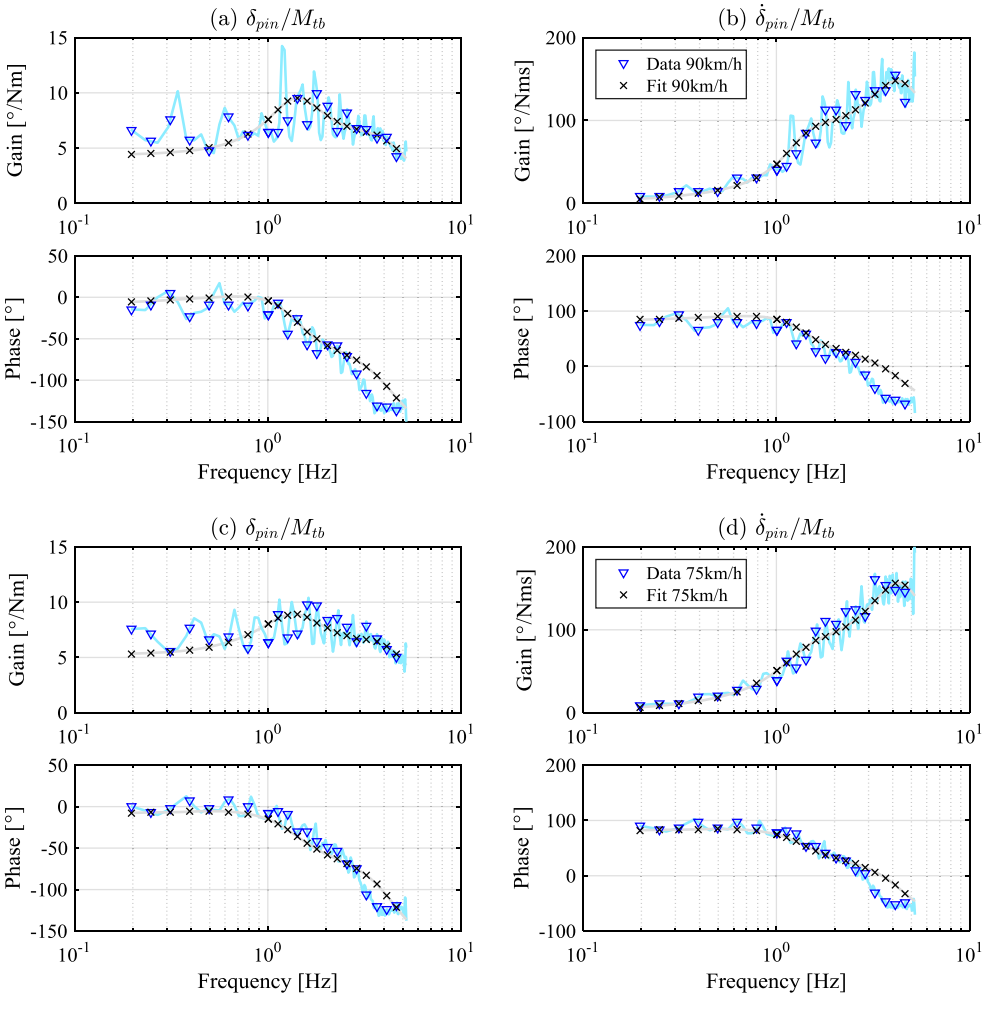

Figure 7. Pinion frequency response at $v_x = 90$ km/h (a and b) and 75 km/h (c and d) in terms of torsion bar torque to pinion angle and angular velocity respectively. The effective pinon inertia, damping and linearised assist gain are estimated (using previously shown estimated rack force FRF) to fit the measured FRF.

coherence to the measured response. The deviation at lower frequencies is due to the contribution of non-linear basic assistance in the measured FRF. This should be accepted because the purpose of this step is to identify the transient parameters (for high frequency response). The estimated parameters ($\hat{J}_{\text{ref}}$, $\hat{b}_{\text{ref}}$ and $\hat{k}_{\text{gain}}$) from Equation (4) are given in Table 2. Relevant observations are as follows:

(1) The estimated reference pinion inertia is lowest at 15 km/h. A similar behaviour was observed on the steering test rig in a separate test, as $\hat{J}_{\text{ref}}$ was minimum at 0 km/h. For $v_x > 60$ km/h, the variance in $\hat{J}_{\text{ref}}$ is lower. However for $v_x \in [30, 60]$ km/h, higher $\hat{J}_{\text{ref}}$ values are as a result of the propagated effect from higher $\hat{\sigma}_{\alpha_f}$ values. This shortcoming is due to the magnitude deviation (above 3 Hz) between the estimated and measured

Table 2. Frequency response estimated parameters at different vehicle speeds: pinion inertia, pinion damping, linearised assist gain, steering trail, front and rear axle tyre relaxation length, front and rear axle tyre cornering stiffness and vehicle yaw inertia.

v_x (km/h)	$\hat{J}_{\text{ref}}$ (kgm^2)	$\hat{b}_{\text{ref}}$ (Nms/rad)	$\hat{k}_{\text{gain}}$ (−)	$\hat{n}_t$ (m)	$\hat{\sigma}_{\alpha_{\text{f}}}$ (m)	$\hat{\sigma}_{\alpha_{\text{r}}}$ (m)	$\hat{C}_{\alpha_{\text{f}}}$ (N/rad)	$\hat{C}_{\alpha_{\text{r}}}$ (N/rad)	$\hat{J}_z$ (kgm^2)
105	0.0512	1.077	2.102	0.0817	0.0328	0.3565	134740	161910	3007
90	0.0601	1.068	2.475	0.0827	0.0273	0.3364	135660	160840	3214
75	0.0613	1.006	2.647	0.0838	0.0313	0.3666	138080	159010	3299
60	0.0779	0.552	2.538	0.0845	0.3061	0.3223	142110	155750	3114
45	0.0905	0.128	2.469	0.0909	0.2897	0.3138	145012	151020	3062
30	0.0774	−0.583	1.484	0.1022	0.1150	0.3649	145012	151020	3020
15	0.0487	−1.242	0.599	0.1594	0.0252	0.3818	145012	151020	3005

rack force FRF. It is caused by the vehicles' semi-active suspension control function (or basically suspension compliance), preventing higher roll rates in this frequency range. Thus creating a substantial effect in the actual rack force signal.

(2) Although the estimated reference pinion damping clearly increases from 15 to 105 km/h, but it shows a saturating trend with increasing v_x. The interesting point is negative damping for $v_x < 45$ km/h. This is due to the heavily damped vehicle response at lower speeds, which subsequently creates a higher equivalent pinion damping via the rack force response. Even with $\hat{b}_{\text{ref}} < 0$, the overall system damping is positive and hence exhibits stable behaviour. It is evident from the eigenvalues (with estimated parameters in **A**) of Equation (10) in complex left half plane (LHP). This implies, with $\hat{b}_{\text{ref}} < 0$, the overall steering damping is reduced at lower vehicle speeds for an acceptable steering feedback to the driver. Simultaneously the estimated linearised assist gain also drops at lower speeds, because the steering rack (or pinion) stiffness reduces.

(3) The estimated total steering trail, $\hat{n}_t$, shows a consistent result for $v_x > 30$ km/h. However, the value increases at lower speeds for a good correlation with the measured rack force FRF. This behaviour can be attributed to the effects of suspension compliance. Also during optimisation, $\hat{J}_z$ was ensured to have a lower deviation (i.e. within ±5%) about its theoretical value (≈3150 kgm^2).

The estimated parameters were finally validated with the measurements on the steering wheel, i.e. in terms of $\delta_{\text{s}}/M_{\text{s}}$. The complete steering system matrices can be obtained using Equation (12) with the modified steering wheel dynamics from Equation (2), $M_{\text{s}}(t) = (J_{\text{s}} + J_{\text{rob}})\ddot{\delta}_{\text{s}}(t) + b_{\text{s}}\dot{\delta}_{\text{s}}(t) + M_{\text{tb}}(t)$. The actual system input is M_{s} and the other parameters are already known. These results also cohered with the measured FRF of $\delta_{\text{s}}(i\omega_n)/M_{\text{s}}(i\omega_n)$.

The steady-state pinion response results are presented in Figure 8(b and c) respectively for 90 and 75 km/h. K_{assist} (or basic assistance) function is derived at first using the on- and off-centre pinon stiffness as mentioned in Section 3.5.1. And then the Coulomb friction torque (on the pinion) to fit the hysteresis. Table 3 lists the estimated values $\hat{c}_{\text{pin,on}}$, $\hat{c}_{\text{pin,off}}$ and $\hat{M}_{\text{fric,C}}$ with the following observations:

(1) The steady-state steering rack stiffness (at 0.2 Hz) increases with vehicle speed (e.g. Figure 6); thereby it directly relates to $\hat{c}_{\text{pin,on}}$. The relation is almost linear with v_x. The

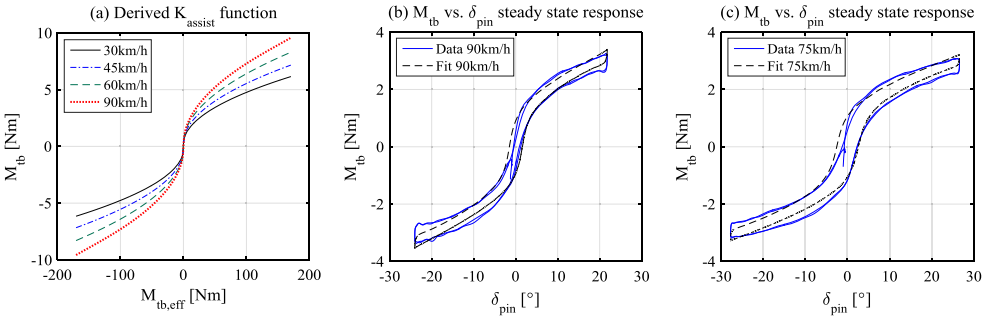

Figure 8. (a) Derived K_{assist} function to replicate the basic assistance within linear vehicle handling range at different speeds. Steady-state pinion response at $v_x = 90$ km/h (a) and 75 km/h (b) respectively. The fitted model and measurement data have been compared, showing a good estimation of the non-linear friction and basic assistance.

Table 3. Steady-state response estimated parameters at different vehicle speeds: on-centre, off-centre pinion stiffness and Coulomb friction torque.

v_x (km/h)	$\hat{c}_{pin,on}$ (Nm/rad)	$\hat{c}_{pin,off}$ (Nm/rad)	$\hat{M}_{fric,C}$ (Nm)
105	53.326	16.160	2.962
90	44.452	10.541	2.703
75	35.482	6.979	2.494
60	25.911	4.179	2.312
45	18.765	1.735	2.113
30	10.903	0.512	1.875
15	6.045	0	–[a]

Note: [a]Discarded due to high steering angle value.

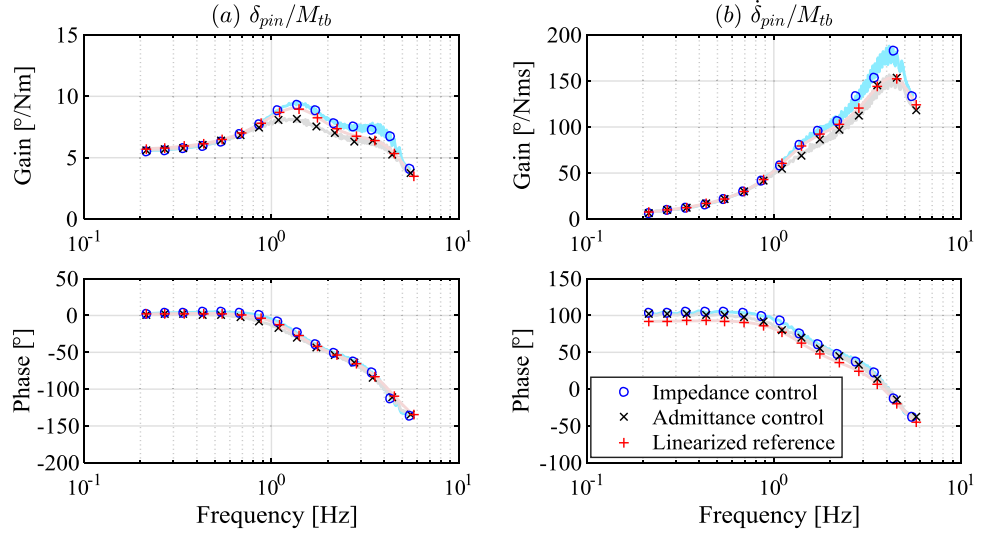

Figure 9. Frequency response of torsion bar torque to (a) pinion angle and (b) angular velocity for EPAS (derived from CarMaker) using impedance and admittance control respectively without non-linear functions. 'Linearised reference' exhibits the estimated response from Section 3.4.3 (excluding basic assist and friction).

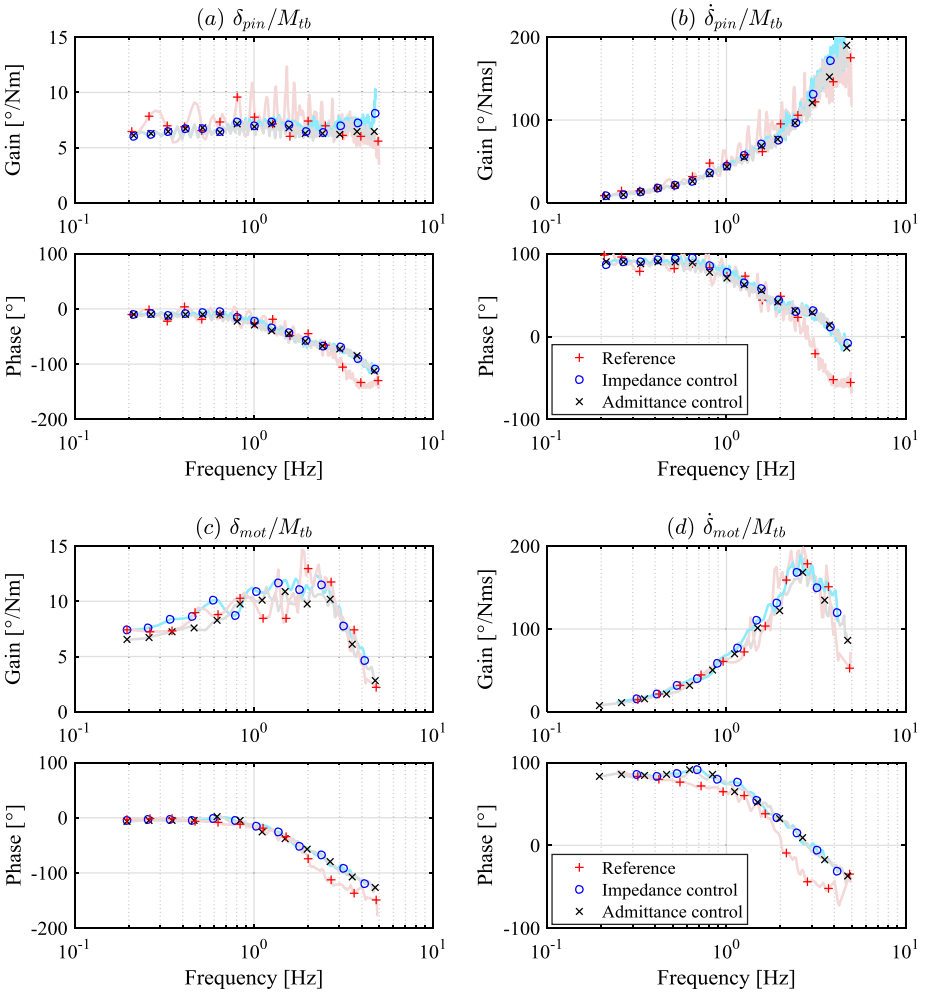

Figure 10. Frequency response of torsion bar torque to (a) pinion angle and (b) angular velocity for EPAS (derived from CarMaker) using impedance and admittance control respectively with the complete reference model. Real-time SbW-FFb frequency response result in terms of torsion bar torque to (c) motor angle and (d) angular velocity with the complete reference model. Both 'Reference' FRF were measured from the vehicle.

contribution of K_{assist} (see Figure 8a) is to make the transition from $c_{\text{pin,on}}$ to $c_{\text{pin,off}}$. With increasing v_x, $\hat{c}_{\text{pin,off}}$ shows a non-linear progressive characteristic (basically a byproduct of the basic assistance function).

(2) The steering hysteresis reduces with increasing v_x, comparing Figure 8(b and c), thus signifying the drivers' preference. However $\hat{M}_{\text{fric,C}}$ increases with v_x (almost linearly), refer Table 3, since the estimation included the basic assistance during optimisation (see Section 3.5.2 and Figure 2b). With the given reference generator layouts, higher effective (total) steering pinion friction is required with increasing v_x. Moreover at a given v_x, the on-centre friction torque is higher than the off-centre friction torque due to the non-linear basic assist function.

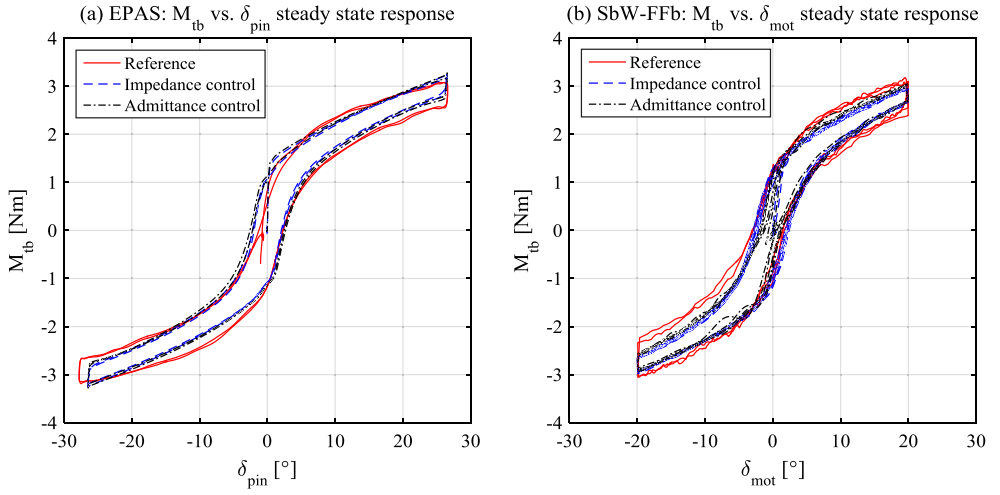

Figure 11. (a) CarMaker result of steady-state steering response in terms of torsion bar torque versus pinion angle for EPAS. (b) Real-time SbW-FFb response in terms of torsion bar torque versus feedback motor angle.

4.2. Validation of the reference generator

The implementation of the impedance and admittance control reference generator has been shown here using the estimated parameters as mentioned in Tables 2 and 3. In impedance control, the torque reference is used by the feedback controller to minimise the torque error and vice versa in admittance control for angular position. The feedback controllers ensured stability and performance as derived in [9,13,15]. For EPAS, the results have been generated using a validated vehicle model, including steering and motor models (with a motor current control). Refer Figure 9, for torsion bar torque to (a) pinion angle and (b) angular velocity FRF at 75 km/h. The linearised reference in this figure is derived in Section 3.4.3 and shown earlier in Figure 7. The results signify an appropriate execution of the reference generator (excluding non-linear basic assistance and friction model) with a sufficient feedback controller performance.

In the final step, the complete reference generators including basic assistance and friction are implemented. The simulation results are presented in Figure 10(a and b) for EPAS. The reference in this case is the measured FRF from the vehicle. The response can be found marginally more damped. Similarly for SbW-FFb,[1] the test rig FRF results from impedance and admittance control are shown in Figure 10(c and d). The feedback motor angle (δ_{mot}) in SbW-FFb is equivalent to δ_{pin} from EPAS. As the presented approach holds, therefore the results show close proximity to the measured FRF from the vehicle ('Reference' with red-coloured 'plus' markers in Figure 10). The steady-state steering response results at 75 km/h are also shown in Figure 11(a and b) for EPAS and SbW-FFb respectively. The figure shows close tracking of the reference (with a good hysteresis correlation), which holds true for all the vehicle speeds not shown here. This indicates that the developed reference generators could reproduce the actual steering response in an effective manner.

5. Conclusion

This paper has presented an approach to extract a steering feedback reference model from an existing vehicle. For this, the steering response identification is done using the conventional open-loop driving manoeuvres on a typical steering system. The identification captures the cumulative influence of the hardware and control software. An inertia-spring-damper-friction model is fitted at different vehicle speeds to objectify the drivers' haptic feedback. The inertia and damping parameters are identified using the frequency response. This requires the frequency response function estimate of steering rack displacement to rack force, which is derived at first from the vehicle response. The estimated rack force frequency response function at higher vehicle speeds showed a good coherence to the actual measurement, but it certainly needs improvement in the future for lower speeds by including the un-modelled effects such as suspension compliance, jacking force and tyre scrub moment. Lastly, the non-linear spring stiffness and friction parameters are identified from the steady-state response. This defines the typical steering hysteresis characteristic. Since the model is based on the vehicle measurements with driver-in-the-loop, therefore the contribution of the (hands-off) active return function is excluded and considered out of scope. The identified reference models can be used for both closed-loop electric power assisted steering and steer-by-wire force-feedback systems in admittance (or position) and impedance (or torque) control settings.

The resulting reference model has parameters with intuitive interpretations, which could provide an easy steering feedback tuning in the future. It is limited to the driver as an excitation source and does not account for an actual road excitation. As a result, the driver feels a virtual steering feedback depending on the tyre–road conditions of the identification measurements. This is the current limitation, but inevitably it is the first step towards the closed-loop haptic feedback control. The inclusion of road excitation in the reference model requires an estimated (or actual) real-time steering rack force signal. This will be considered separately in the future work. Also, the architecture of the haptic feedback reference model provided in this paper is qualitatively valid for other closed-loop force-feedback systems such as telerobotics, exoskeleton, and so on.

Note

1. The reference generator implemented here has been derived using manually excited measurements and not by steering robot with an exactly similar approach as in Section 3. Also, the tyre relaxation effect was excluded.

Acknowledgments

The authors would like to thank Professor Bengt Jacobson from Chalmers University of Technology, Pontus Carlsson, David Dahlgren and Joakim Norrby from Volvo Car Corporation for the technical discussions.

Disclosure statement

No potential conflict of interest was reported by the authors.

Funding

The authors are thankful to the ITEAM project in the European Union's Horizon 2020 research and innovation program under Marie Sklodowska-Curie grant agreement no. 675999 and VINNOVA of the Fordonsstrategisk forskning och innovation (FFI), Steer-by-Wire Opportunities, Performance and System Safety (SWOPPS) project [grant no. 2017–05504].

Nomenclature

J_{sys}	System inertia
b_{sys}	System viscous damping
c_{sys}	System stiffness
μ_{sys}	System coefficient of friction
M	Input torque
M_{fric}	Friction torque
J_s	Steering inertia
J_{rob}	Steering robot inertia
b_s	Steering viscous damping
b_{tb}	Torsion bar viscous damping
c_{tb}	Torsion bar stiffness
J_{pin}	Pinion inertia
b_{pin}	Pinion viscous damping
c_{pin}	Pinion stiffness
J_{comp}	Compensating inertia
b_{comp}	Compensating viscous damping
J_{ref}	Reference pinion inertia
b_{ref}	Reference pinion viscous damping
c_{rack}	Steady-state steering rack stiffness at 0.2 Hz
$c_{pin,on}$, $c_{pin,off}$	Pinion on- and off-centre stiffness
c_{fric}	Pinion friction model stiffness
k_{gain}	Linearised basic assist gain
K_{assist}	Basic assist function
σ	Fitting parameter of Gaussian function
M_s	Steering torque
M_{tb}	Torsion bar torque
$M_{pin,dyn}$	Pinion dynamic torque
$M_{tb,eff}$	Effective torsion bar torque after basic assistance
$M_{s,fric}$	Steering friction torque
$M_{comp,fric}$	Compensating friction torque
M_{rack}	Equivalent pinion torque due to steering rack force
$M_{tb,fric}$	Torsion bar friction torque
$M_{ref,fric}$	Reference torsion bar friction torque
$M_{fric,C}$	Torsion bar Coulomb friction torque
M_{mot}	Motor torque
$M_{mot,eff}$	Effective motor torque
v_x, v_y	Vehicle longitudinal and lateral speed
a_y	Vehicle lateral acceleration

F_{rack}	Steering rack force
n_t	Steering trail (or sum of caster and tyre pneumatic trail)
$\dot{\psi}$	Vehicle yaw rate
β	Body sideslip angle
$\alpha_{\text{f}}, \alpha_{\text{r}}$	Front and rear axle lateral slip angle
$C_{\alpha_{\text{f}}}, C_{\alpha_{\text{f}}}$	Front and rear axle tyre cornering stiffness
m	Vehicle mass
J_z	Vehicle yaw inertia
$\sigma_{\alpha_{\text{f}}}, \sigma_{\alpha_{\text{r}}}$	Front and rear axle tyre relaxation length
$l_{\text{f}}, l_{\text{r}}$	Distance from CG to front and rear axle
x_{rack}	Steering rack displacement
$i_{\text{s}}, i_{\text{rp}}, i_{\text{epas}}$	Pinion-to-tyre, rack-to-pinion and motor-to-pinion ratio
$\boldsymbol{\theta}$	Parameter estimation vector
$\boldsymbol{\theta}^-, \boldsymbol{\theta}^+$	Upper and lower bounds of parameter estimation vector
$\hat{\theta}$	Estimated parameter
$J(\theta)$	Objective function
$\mathbf{W}_{\text{m}}, \mathbf{W}_{\text{p}}$	Weighting matrices for FRF magnitude and phase
$\mathbf{N}_{\text{m}}, \mathbf{N}_{\text{p}}$	Normalising matrices for FRF magnitude and phase
$\mathbf{E}_{\text{m}}, \mathbf{E}_{\text{p}}$	Error matrices for FRF magnitude and phase
$w_{\text{mag},y_k}, w_{\text{ang},y_k}$	Weighting gains for kth input–output FRF magnitude and phase
$\hat{H}_{\text{stat},\delta y_k}$	Steady-state input–output FRF gain at 0.2 Hz
s	Laplace operator
ω	Frequency
$\hat{S}_{dy}, \hat{S}_{du}$	Disturbance-output and -input cross spectral densities
$\hat{H}_{uy}$	Input–output FRF
$\hat{\gamma}_{dx}$	Disturbance to signal ' x' coherence
$\mathbf{x}$	System state vector
$\mathbf{y}$	System output vector
$\mathbf{u}$	System input vector
$\mathbf{A}, \mathbf{B}, \mathbf{C}, \mathbf{D}$	State, input-to-state, state-to-output and feedthrough matrices
$\mathbf{Y}(s)$	Laplace transform of system output vector
$Y_k(s)$	Laplace transform of kth system output
$F, H_{\text{m}}, R_{\text{m}}$	Laplace functions
$\mathbf{0}_{n\times n}$	n by n null matrix
$\mathbf{I}_{n\times n}$	n by n identity matrix
$\delta, \dot{\delta}, \ddot{\delta}$	Angular position, velocity and acceleration
$\delta_{\text{s}}, \dot{\delta}_{\text{s}}, \ddot{\delta}_{\text{s}}$	Steering angle, velocity and acceleration
$\delta_{\text{pin}}, \dot{\delta}_{\text{pin}}, \ddot{\delta}_{\text{pin}}$	Pinion angle, velocity and acceleration
$\delta_{\text{mot}}, \dot{\delta}_{\text{mot}}$	Feedback motor angle and velocity
δ_{tyre}	Tyre or wheel angle

ORCID

T. Chugh http://orcid.org/0000-0001-8587-9912
M. Klomp http://orcid.org/0000-0001-5972-1660
B. Shyrokau http://orcid.org/0000-0003-4530-8853

References

[1] Marban A, Casals A, Fernandez J. Haptic feedback in surgical robotics: Still a challenge. In: Armada M, Sanfeliu A, Ferre M, editors. ROBOT2013: First Iberian Robotics Conference. Advances in Intelligent Systems and Computing Vol. 252. Cham: Springer; 2014.

[2] Okamura AM. Haptic feedback in robot-assisted minimally invasive surgery. 2008.

[3] Lawrence DA. Stability and transparency in bilateral teleoperation. IEEE Trans Rob Autom. 1993;9(5):624–637.

[4] Defaÿ F, Alazard D, Antraygue C. Impedance active control of flight control devices. IEEE/ASME International Conference on Advanced Intelligent Mechatronics. AIM; 2010. p. 335–340.

[5] Bolopion A, Régnier S. A review of haptic feedback teleoperation systems for micromanipulation and microassembly. IEEE Trans Autom Sci Eng. 2013;10(3):496–502.

[6] Wildenbeest JG, Kuiper RJ, Van Der Helm FC. Position control for slow dynamic systems: haptic feedback makes system constraints tangible. Conference Proceedings – IEEE International Conference on Systems, Man and Cybernetics; 2014 Jan; San Diego, CA, USA. 2014. p. 3990–3995.

[7] Rehnmark ROA, Aldridge H, Askew RS, et al. Robonaut : NASA's space humanoid. IEEE Intell Syst Appl. 2000;15(4):57–63.

[8] Kosuge K, Fujisawa Y, Fukuda T. Control of mechanical system with man-machine interaction; 1992;(c). p. 87–92.

[9] Chugh T. Haptic feedback control methods for steering systems [Licentiate thesis]. Chalmers University of Technology; 2019.

[10] Harrer M, Pfeffer P. Steering handbook. Weissach: Springer International Publishing AG; 2017.

[11] Chugh T, Chen W, Klomp M. Design and control of model based steering feel reference in an electric power assisted steering system. 25th IAVSD Symposium on Dynamics of Vehicles on Roads and Tracks; Rockhampton, Queensland, Australia. 2017. p. 43–49.

[12] Düsterloh D, Uselmann A, Scherhaufer J, et al. Objectification of the feedback behavior of the suspension and steering system. 9th International Munich Chassis Symposium. Springer Fachmedien Wiesbaden; 2018.

[13] Chugh T, Bruzelius F, Klomp M. Design of haptic feedback control for steer-by-wire. 21st IEEE International Conference on Intelligent Transportation Systems (ITSC); Maui, HI, USA. 2018. p. 1737–1744.

[14] Hsu H, Harrer M. The new steering system in the 911 porsche carrera – optimized design of a steering system for sportcars; 2012.

[15] Chugh T, Bruzelius F, Klomp M. Comparison of steering feel control strategies in electric power assisted steering. 14th International Symposium on Advanced Vehicle Control (AVEC); 2018 July; Beijing, China. 2018.

[16] Aguirre-Ollinger G, Colgate JE, Member S, et al. Inertia compensation control of a one-degree-of-freedom exoskeleton for lower-limb assistance: initial experiments. IEEE Trans Neural Syst Rehabil Eng. 2012;20(1):68–77.

[17] Bajcinca N, Cortesao R, Hauschild M. Haptic control for steer-by-wire systems. IEEE International Conference on Intelligent Robots and Systems; 2003 October; Las Vegas, NV, USA. 2003. p. 2004–2009.

[18] Katzourakis DI, Abbink DA, Happee R, et al. Steering force feedback for human–machine interface automotive experiments. IEEE Trans Instrum Meas. 2011;60:32–43.

[19] Schouten AC, de Vlugt E, van Hilten JJB, et al. Design of a torque-controlled manipulator to analyse the admittance of the wrist joint. J Neurosci Methods. 2006;154(1–2):134–141.

[20] Brocker M. New control algorithms for steering feel improvements of an electric powered steering system with belt drive. Vehicle Syst Dyn. 2006;44(SUPPL. 1):759–769.

[21] Badawy A, Zuraski J, Bolourchi F, et al. Modeling and analysis of an electric power steering system. International Congress and Exposition Detroit; Michigan; 1999 Mar 1–4. 400. 1999;1999(724).

[22] Hu TH, Yeh CJ, Ho SR. Design of control logic and compensation strategy for electric power steering systems. 2008 IEEE Vehicle Power and Propulsion Conference; VPPC 2008; Harbin, China. 2008. p. 1–6.
[23] Fankem S, Müller S. A new model to compute the desired steering torque for steer-by-wire vehicles and driving simulators. Vehicle Syst Dyn. 2014;52(1):251–271. Available from: https://doi.org/10.1080/00423114.2014.896469.
[24] Hayama R, Kawahara S, Nakano S, et al. Resistance torque control for steer-by-wire system to improve human–machine interface. Vehicle Syst Dyn. 2010;48(9):1065–1075. Available from: https://doi.org/10.1080/00423110903267405.
[25] Balachandran A, Gerdes JC. Designing steering feel for steer-by-wire vehicles using objective measures. IEEE ASME Trans Mechatron. 2015;20(1):373–383.
[26] Kim JH, Song JB. Control logic for an electric power steering system using assist motor. Mech J Int Fed Autom Control (IFAC). 2002;12(3):447–459. Available from: https://doi.org/10.1016/S0957-4158(01)00004-6.
[27] Lee D, Yi K, Chang S, et al. Robust steering-assist torque control of electric-power-assisted-steering systems for target steering wheel torque tracking. Mech J Int Fed Autom Control (IFAC). 2018;49:157–167. Available from: https://doi.org/10.1016/j.mechatronics.2017.12.007.
[28] Williams DE. Synthetic torque feedback to improve heavy vehicle drivability. Proc Inst Mech Eng Part D. 2009;223(12):1517–1527.
[29] Li Y, Shim T, Wang D. Enhancement of steering feel of electric power assist steering system using modeling reference control. 2018 Proceedings of the American Control Conference; 2018 June; Milwaukee, Wisconsin, USA. 2018. p. 3257–3262.
[30] Marouf A, Sentouh C, Djemai M. Control of an electric power assisted steering system using reference model. Proceedings of the IEEE Conference on Decision and Control; Orlando, FL, USA. 2011. p. 6684–6690.
[31] Yang T. A new control framework of electric power steering system based on admittance control. IEEE Trans Control Syst Technol. 2015;23(2):762–769.
[32] ISO 7401:2011(E). Road vehicles – lateral transient response test methods – open-loop test methods. International Standard; 2011.
[33] Katzourakis DI, Abbink DA, Velenis E, et al. Driver's arms' time-variant neuromuscular admittance during real car test-track driving. IEEE Trans Instrum Meas. 2014;63(1):221–230.
[34] Von Groll M, Mueller S, Meister T, et al. Disturbance compensation with a torque controllable steering system. Vehicle Syst Dyn. 2006;44(4):327–338.
[35] Hogan N, Buerger SP. Robotics and automation handbook, chapter 19 impedance and interaction control. Boca Raton (FL): CRC Press, LLC; 2005.
[36] Lampaert V, Swevers J, Al-Bender F. Impact of nonlinear friction on frequency response function measurements. 25th Proceedings of ISMA; Leuven, Belgium. 2000.
[37] Ljung L. System identification: theory for the user. Upper Saddle River (NJ): Prentice Hall PTR; 1999.
[38] Canudas de Witt C, Olsson H, Member S, et al. A new model for control of systems with friction. IEEE Trans Automat Contr. 1995;40(3):419–425.